DSFE: Decoding EEG-Based Finger Motor Imagery Using Feature-Dependent Frequency, Feature Fusion and Ensemble Learning

Kun Yang, Ruochen Li, Jing Xu, Li Zhu, Wanzeng Kong, and Jianhai Zhang

***Abstract*—Accurate decoding finger motor imagery is essential for fine motor control using EEG signals. However, decoding finger motor imagery is particularly challenging compared with ordinary motor imagery. This paper proposed a novel EEG decoding method of feature-dependent frequency band selection, feature fusion, and ensemble learning (DSFE) for finger motor imagery. First, a feature-dependent frequency band selection method based on correlation coefficient (FDCC) was proposed to select feature-specific effective bands. Second, a feature fusion method was proposed to fuse different types of candidate features to produce multiple refined sets of decoding features. Finally, an ensemble model using the weighted voting strategy was proposed to make full use of these diverse sets of final features. The results on a public EEG dataset of five fingers motor imagery showed that the DSFE method is effective and achieves the highest decoding accuracy of 50.64%, which is 7.64% higher than existing studies using exactly the same data. The experiments further revealed that both the effective frequency bands of different subjects and the effective frequency bands of different types of features are different in finger motor imagery. Furthermore, compared with two-hand motor imagery, the effective decoding information of finger motor imagery is transferred to the lower frequency. The idea and findings in this paper provide a valuable perspective for understanding fine motor imagery in-depth.**

***Index Terms*—EEG, finger motor imagery, frequency band selection, feature fusion, ensemble learning.**

Manuscript received 21 November 2023; revised 22 March 2024; accepted 26 April 2024. Date of publication 6 May 2024; date of current version 7 August 2024. This work was supported in part by the Key Research and Development Project of Zhejiang Province under Grant 2020C04009, Grant 2023C03026, Grant 2021C03001 and Grant 2021C03003, in part by the National Natural Science Foundation of China under Grant U20B2074 and Grant 62301196, in part by the Zhejiang Provincial Natural Science Foundation of China under Grant LQ24F020035, in part by Zhejiang Gongshang University 'Digital Interdiscrplinary Construction Management Project' under Grant SZJ2022C007, and in part by the Key Laboratories of Sensing and Application of Intelligent Optoelectronic System in Sichuan Provincial Universities under Grant ZNGD2217. *(Kun Yang and Ruochen Li are co-first authors.) (Corresponding author: Jianhai Zhang.)*

Kun Yang, Ruochen Li, Li Zhu, Wanzeng Kong, and Jianhai Zhang are with the School of Computer Science and Technology, Hangzhou Dianzi University, Hangzhou 310005, China, and also with the Key Laboratory of Brain Machine Collaborative Intelligence of Zhejiang Province, Hangzhou 310018, China (e-mail: yangkun@hdu.edu.cn; jhzhang@hdu.edu.cn).

Jing Xu is with the School of Statistics and Mathematics, Zhejiang Gongshang University, Hangzhou 310005, China.

Digital Object Identifier 10.1109/JBHI.2024.3395910

I. Introduction

BRAIN computer interfaces (BCI) establish direct communication between the human brain and external devices [1]. It allows users to use brain activity and neural information to control devices such as prosthetics, wheelchairs and computers [2]. Motor imagery refers to the thought process by which a person imagines a specific action without actually performing it [3], which is an important research paradigm in the field of BCI. Motor imagery-based BCIs can control external devices to perform appropriate actions by recognizing the user's movement intention [4]. This technology can indirectly assist people with severe movement disorders to restore motor function. At present, research on motor imagery mainly focuses on large-scale limb movements, such as the movements of the left hand, right hand, left foot, right foot, both feet and tongue [5], and there are few studies on fine motor imagery tasks such as finger movements. Fingers are necessary for grasping and moving objects and are closely related to our daily lives. Therefore, studying finger motor imagery is essential to realize the fine motor control of EEG signals and improve the daily life of patients with movement disorders.

Decoding finger movements using EEG is a difficult task. Due to the volume conduction effect of EEG, the signal has a certain degree of aliasing and attenuation [6]. Current research on decoding finger movements using EEG signals mainly adopts machine learning methods based on feature engineering [7], [8], [9], [10], [11], [12], [13], [14]. For example, Quandt et al. [7] studied the EEG of 13 subjects performing four finger movements (excluding ring finger). They used the time series after downsampling as features and used SVM for decoding, achieving a classification accuracy of 43%. Salyers et al. [10] found that the classifier based on mu rhythm (8–13 Hz) had no significant recognition performance on ring finger, but slow cortical potentials (0–5 Hz) decoded ring finger best, while the situation of index finger was almost opposite. They hypothesized that slow cortical potentials and mu rhythm act in independent but complementary ways on the task of recognizing finger movements. Kaya et al. [11] published an EEG dataset of 8 subjects performing five finger motor imagery task in 2018, and they used 0–5 Hz Fourier transform amplitudes features and SVM to decode them, achieving 43% accuracy. Kato [13] and Azizah [14] conducted experiments on the dataset published by kaya using multi-class CSP features and spectrogram features, respectively. Some studies have achieved good results using deep

learning techniques to decode finger motor imagery, such as multilayer perceptron [15] and LSTM [16]. There are also some studies that use high-density EEG electrodes to decode finger movements [17], [18]. Due to the limited interpretability of deep learning, traditional machine learning methods still remain a focal point of our research.

Some studies have shown that selecting a specific frequency band for each subject can improve the decoding performance of ordinary motor imagery tasks [19], [20]. However, the previous studies of fine motor imagery targeting different fingers did not consider the frequency band difference of the subjects. We speculate that for a fine task such as finger motor imagery, the effective frequency band might be different for different subjects. Due to the instability and non-linearity of EEG signals, it is difficult for a single type of features to provide sufficient decoding information, so different types of features should be used in EEG decoding. We also hypothesise that the effective frequency bands of different features would be different. It is necessary to identify feature-dependent effective frequency bands for candidate features.

Previous work has investigated frequency band selection for ordinary motor imagery tasks (e.g., left hand, right hand, feet, tongue). For example, Rodriguez et al. [21] proposed a method of the spectrogram based short-time Fourier transform (SSTFT) to select subject-specific frequency bands for each subject in the pedal motor imagery task. However, the SSTFT method was designed around two metrics (i.e. sparseness constraint and total power) and independent of specific features. In other words, the frequency bands selected by the SSTFT method are likely to be invalid for a specific feature. On the other hand, their method needs to optimize several parameters, which is time-consuming. In a recent work, Wu et al. [22] proposed a discriminative and multi-scale filter bank (DMFB) algorithm to select a specific frequency band for each subject, which was applied to the motor imagery dataset of left hand, right hand, tongue, and feet. Their method first calculated the F-statistic of the covariance matrix of EEG signals in different sub-frequency bands, and then selected the frequency band according to the F-statistic. Similarly, this method also ignored the difference in effective frequency bands between different features, i.e., the frequency band selection was independent of features. In addition, the calculation of the F-statistic based on the Riemannian distance of this method is very time-consuming. Maria et al. [23] proposed a class-distinctiveness based band selection method, which selected bands based on the classDis value of the covariance matrix of each sub-band. Like the previous two methods, this approach is also feature-independent.

In this study, we proposed a novel decoding method using feature-dependent frequency band selection, feature fusion and ensemble learning (DSFE) for fine finger motor imagery. On a publicly available EEG data of five fingers motor imagery task [11], the proposed DSFE method has been evaluated from several perspectives. First, our method of feature-dependent frequency band selection based on correlation coefficient (FDCC) has been compared with two previous frequency band selection methods of SSTFT [21] and DMFB [22]. Then, the effectiveness of feature fusion and ensemble learning has been investigated. Moreover, our final decoding result has been compared with the results of related studies on the same dataset. The experimental results show that: (1) all methods of feature-dependent frequency band selection, feature fusion, and ensemble learning can effectively improve the decoding performance of finger motor imagery; (2) the proposed DSFE method has achieved a final average decoding accuracy of 50.64%, which is at least higher 7.64% than those of existing studies on the exact same data. The experiments in this paper further reveal that the effective frequency bands of different types of features are different in finger motor imagery. Through careful analysis, it is found that there is a distinct difference between the effective frequency bands of finger motor imagery and those of two-hand motor imagery. Compared with two-hand motor imagery, the effective decoding information of finger motor imagery is transferred to the lower frequency. The idea and interesting findings in this paper provide a valuable perspective for understanding fine motor imagery.

The contributions of this paper can be summarized as follows.

1) To the best of our knowledge, the novel concept of feature-dependent effective frequency band has been proposed for the first time, and a FDCC method is proposed to automatically identify effective frequency bands for each type of feature. This study demonstrated that the effective frequency bands of different types of features are indeed different in finger motor imagery.
2) A feature fusion method based on ReliefF has been proposed for fusing the Fourier transform amplitude features (FTA) and the Riemannian geometry features (RG) to produce different refined sets of decoding features.
3) After the stage of frequency band selection and feature fusion, multiple effective feature sets are obtained. An ensemble learning model using the weighted voting strategy has been proposed to make full use of these diverse sets of final decoding features.
4) The proposed methods improve the interpretation and discrimination ability of feature and can provide very valuable information for an in-depth study of the characteristics of EEG signals of specific task. The methods revealed that the effective decoding information of finger motor imagery is transferred to the lower frequency compared with two-hand motor imagery. This finding suggests that there may be a great difference in the internal mechanism between finger motor imagery tasks and two-hand motor imagery.

II. Methodology

Fig. 1 showed the graphical framework of the proposed DSFE method for decoding finger motor imagery, which comprises three main steps: feature-dependent effective frequency band selection, feature fusion, and ensemble learning. In the first step of the DSFE method, the FDCC method was proposed to select effective frequency bands of specific feature. In the second step, the FTA feature and the RG feature were extracted from the effective frequency bands to save as two types of candidate features, then a feature fusion method based on ReliefF was

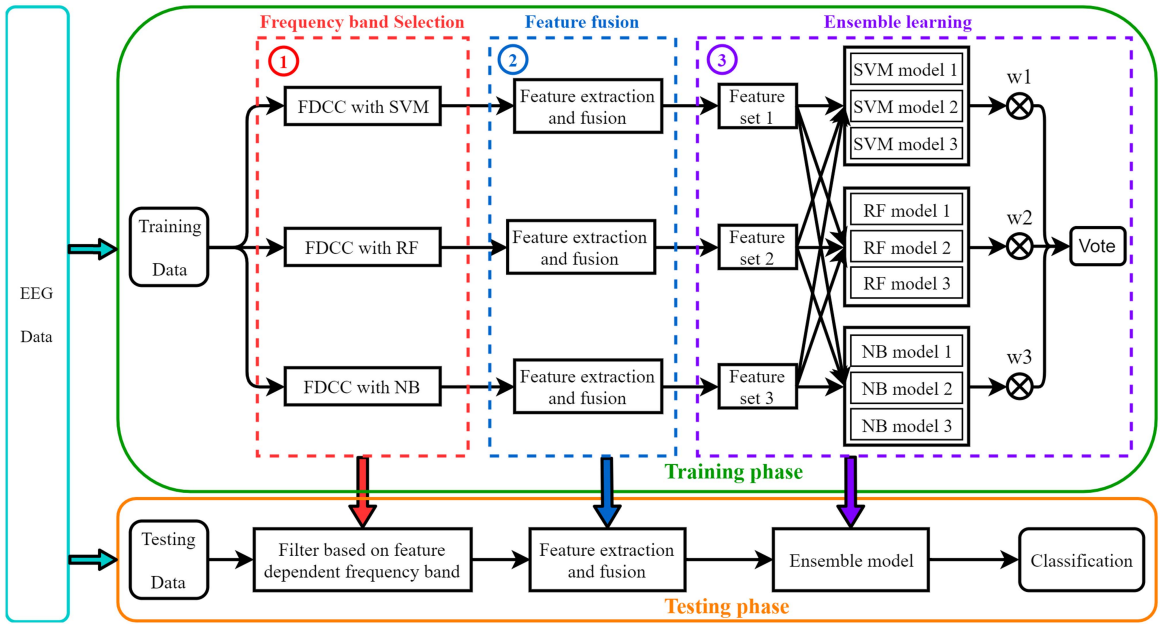

Fig. 1. The graphical framework of the proposed DSFE method, which consists of a training phase and a testing phase. The training phase consists of three sequential steps: (1) frequency band selection, (2) feature fusion and (3) ensemble learning. Based on the feature-dependent effective frequency band identified by the proposed FDCC method in the first step, the candidate features are extracted and then fused to produce several refined sets of discriminative features. These refined sets of discriminative features serve as input to the ensemble learning in the third step.

proposed to remove redundant features and produce multiple effective and refined sets of discriminative features. Finally, an ensemble model based on different refined sets of discriminative features was proposed, which integrated the prediction results of several base classifiers by using a weighted voting strategy.

A. Discriminative Features

Inspired by previous studies [11], [24], two types of features were extracted for decoding EEG signals. One was the FTA feature of the EEG signals, which represented the information possessed by each EEG channel. The other was the RG feature, which reflected the interaction information between the channels.

1) FTA Features: FTA features were proposed by Kaya et al. [11]. To extract FTA features, the discrete Fourier transform was first applied to the EEG signal of each channel. Then, for a given frequency range $[f_1, f_2]$ Hz, the Fourier transform amplitudes of all frequency components in the range were extracted and converted to real numbers. This allowed us to obtain an amplitude vector for each channel. The amplitude vectors of all channels were concatenated into one vector as the final FTA features.

2) RG Features: Barachant et al. [24] proposed the Riemannian geometry classification framework in 2012. It included the minimum distance to Riemannian mean (MDRM) method and the tangent space linear discriminant analysis (TSLDA) method. In the Riemannian framework, the distance between different neural states was represented by the sample covariance matrix. We mapped the sample covariance matrix into the Riemannian tangent space and extracted the RG features via matrix vectorization. Specifically speaking, for a given frequency range $[f_1, f_2]$ Hz, a fourth-order Butterworth filter was used to bandpass filter the EEG signals. Then for a multi-channel EEG signal $X \in R^{n\times m}$, its sample covariance matrix P was calculated:

$$P = \frac{1}{m-1} XX^T \tag{1}$$

where m is the number of sampled points in EEG trial X, n is the number of channels. Next, the Riemannian mean reference matrix $P_{\mathfrak{G}}$ was computed using the Riemannian geodesic distances for the sample covariance matrices in the training set. The Riemannian distance from the sample covariance matrix to the reference matrix was then calculated. Finally, mapping the Riemannian distance into the tangent space and vectorizing it, a Riemannian geometry feature vector of dimension $n \times (n+1)/2$ was obtained as follows:

$$s = upper(\log(P_{\mathfrak{G}}^{-\frac{1}{2}} P P_{\mathfrak{G}}^{-\frac{1}{2}})) \tag{2}$$

where $\log(\cdot)$ represents the matrix logarithm, $upper(\cdot)$ consists of keeping the upper triangular part of a symmetric matrix and vectorizing it by applying unit weight for diagonal elements and $\sqrt{2}$ weight for out-of-diagonal elements.

B. Feature-Dependent Frequency Band Selection Based on Correlation Coefficient (FDCC)

Our proposed feature-dependent frequency band selection method was described in Algorithm 1. First, the EEG signal of frequency range $(f_{\text{start}}, f_{\text{end}})$ was decomposed into several non-overlapping subbands of width h Hz. For example, the 0–30 Hz frequency range can produce 15 subbands with a width of 2 Hz, namely 0–2, 2–4, $\cdots$, 26–28, 28–30 Hz. This step was accomplished by bandpass filtering the EEG signal with a

Algorithm 1: The frequency band selection of FDCC.

Input: training data X, training label L, classifier C, frequency range (f_{start}, f_{end}), subband width h;
Output: frequency band (f_{low}, f_{high});
Initialization: $R[\ ]$, $U[\ ]$, $\omega \leftarrow \frac{f_{end}-f_{start}}{h}$;
for $(i \leftarrow 1\ to\ \omega)$ **do**
  $f_1 \leftarrow (i-1)\cdot h,\ f_2 \leftarrow i \cdot h$;
  $features, \alpha \leftarrow CalculateFeatures(X, (f_1, f_2))$;
  // α is the number of features
  $corrlist \leftarrow CalculateCorr(features, L)$;
  // Calculation of correlation coefficients
  $R[i] \leftarrow \frac{1}{\alpha}\sum_{r=1}^{\alpha} |corrlist[r]|$;
end
$R_{sort} \leftarrow ReverseSort(R)$;
for $(T \leftarrow 1\ to\ \omega - 1)$ **do**
  $Threshold \leftarrow R_{sort}[T]$;
  $BandSelect[\ ]$;
  for $(i \leftarrow 1\ to\ \omega)$ **do**
    $BandSelect[i] \leftarrow (R[i] \geq Threshold)\ ?\ 1 : 0$;
  end
  Merging the adjacent selected sub-bands according to $BandSelect$, and get several candidate bands;
  Repeat steps 4-6 to extract features and calculate the coefficient for each candidate band;
  Select the band (f_1, f_2) with the largest coefficient from candidate bands;
  $acc \leftarrow CrossValidation(X, L, (f_1, f_2), C)$;
  $U[T] \leftarrow [f_1, f_2, acc]$;
end
$(f_{low}, f_{high}) \leftarrow FindBand(U, max(U(:, 3)))$;
return (f_{low}, f_{high}).

fourth-order Butterworth filter. Then, features of the candidate type were extracted for each subband of the EEG signal. The Pearson correlation coefficient was calculated for each feature with respect to the sample label. Next, the average absolute correlation coefficient of all features within each subband was calculated and used as the evaluation index for each subband.

All subbands were sorted according to the average values from large to small, and the first T subbands were selected as the valid subbands. The selected subbands were then merged according to whether they were adjacent to each other, and several candidate bands were obtained. For example, after merging the selected 0–2, 2–4, 6–8, 8–10 and 10–12 subbands, two candidate bands 0–4 and 6–12 were obtained. Features of the candidate type were re-extracted for each candidate band, and the average absolute correlation coefficient was calculated in the same way as for each subband. The candidate frequency band with the largest average value was then selected as the final effective frequency band.

As T is related to the specific task data and would affect the final result of the frequency band selection, cross-validation was used to determine the optimal T of specific data. For each possible T value, an effective frequency band can be obtained by the above steps. The corresponding features were then extracted from the EEG signal in this frequency band, so that the average accuracy of 5-fold cross-validation of these features can be calculated. The frequency band corresponding to the T with the highest average accuracy was selected as the final effective frequency band. It should be pointed out that the frequency band selection was performed on the training data, and slightly different effective frequency bands would be obtained by using different classification models.

C. Feature Fusion

FTA features and RG features were used in this paper. FTA features were created from the Fourier transform amplitudes of different EEG channels, reflecting the sum of information from each channel. RG features were computed from the EEG covariance matrix, reflecting the interaction information between channels. We hypothesized that these two types of features are complementary and that their fusion would be more effective in decoding finger motor imagery. The purpose of feature fusion was to remove redundant and interfering features to obtain a refined effective feature set. Features of different types were calculated for the target frequency band and concatenated to form a vector. Then, the ReliefF algorithm was used to eliminate the redundant features in this long vector and the final refined feature set was obtained.

Relief algorithm was proposed by Kira et al. [25]. It assigns different weights to each feature based on the relevance of each feature and class, and then removes the features with weights less than a certain threshold. Such algorithms were initially limited to binary classification problems only. In 1994, Kononeill [26] extended it to obtain the ReliefF algorithm, so that it can deal with multi-class problems. Since the finger motor imagery classification in this work belongs to the five-classification problem, we used the ReliefF algorithm for feature selection. First, assume that the training set is D, the number of iterations is t, the number of classes is N, the number of nearest neighbour samples is v, and the threshold of feature weight is δ. The algorithm first randomly selects a sample S from the training set D, then finds the v nearest neighbour samples $H_j(j = 1, 2, \ldots, v)$ of S from the samples of the same class, and then finds the v nearest neighbour samples $M_j(j = 1, 2, \ldots, v)$ from the samples of different classes with S. For feature A, its weight $W(A)$ is calculated by the following formulas:

$$W(A) = W(A) - \frac{1}{tv}\sum_{j=1}^{v} diff(A, S, H_j) + \frac{1}{tv}\sum_{c(M_j)}^{N}[Q(M_j)\sum_{j=1}^{v} diff(A, S, M_j)] \tag{3}$$

$$Q(M_j) = \frac{\eta(c(M_j))}{1 - \eta(c(S))} \tag{4}$$

$$diff(A, S_1, S_2) = \frac{|S_1[A] - S_2[A]|}{\max(A) - \min(A)} \tag{5}$$

where $c(M_j)$ denotes the class of samples M_j, $c(S)$ denotes the class of sample S, and $c(M_j) \neq c(S)$. $\eta(\cdot)$ represents the proportion of samples in this class among all samples. Equation (5) represents the difference between sample S_1 and S_2 on feature A. $W(A)$ starts at 0 and takes t iterations to update. The weight was calculated for each feature, and then the feature with a weight value less than δ was removed. Feature fusion was implemented using the MATLAB function "relieff" based on "classification" with the number of nearest neighbours samples v set to 20. We kept only the top 25% features with large weights, and this threshold was determined by the effect experiment of selecting different proportions of features on the classification accuracy.

D. Ensemble Learning Model

After frequency band selection and feature fusion, multiple effective feature sets were obtained. To make full use of these diverse feature sets, we proposed an ensemble learning model that combined the predictions of multiple base classifiers using a weighted voting strategy. The ensemble model includes three base classifiers: SVM, RF, and NB. Each base classifier was trained on each feature set, resulting in a total of nine specific classifiers for the final prediction. Since the performance of each classifier was not equal, we assigned a certain weight to each classifier. Based on the prediction results of these nine models, we used a relative majority weighted voting strategy to select the class with the highest probability as the final prediction result.

Suppose there are B classifiers with weight $w_b|_{b=1}^{B}$, $c_k|_{k=1}^{\lambda}$ is the class label, x is the sample to be predicted. The prediction result of x by the b-th classifier is $\{y_b^{c_1}(x), \ldots, y_b^{c_\lambda}(x)\} \in \{0,1\}^{\lambda}$, where $y_b^{c_k}(x) = 1$ if the predicted label is c_k and $y_b^{c_k}(x) = 0$ otherwise $(1 \leq k \leq \lambda)$. Then, the probability that sample x is predicted as c_k by all classifiers is

$$p(c_k) = \sum_{b=1}^{B} y_b^{c_k}(x) w_b. \tag{6}$$

The prediction result of the ensemble model $Y(x)$ is the class with the highest probability.

$$Y(x) = c_{\arg\max_k p(c_k)} \tag{7}$$

We experimentally found that the SVM model performed best and RF performed slightly better than NB. Thus, the weights assigned to each model of SVM, RF and NB were 0.16, 0.09 and 0.08, respectively. Here is an example to illustrate the process of weighted voting. Assuming that the class label set is $\{1,2,3,4,5\}$ and the prediction results of nine classifiers are SVM$\{1,2,1\}$, RF$\{2,3,2\}$, NB$\{4,5,2\}$. After weighted voting, the probabilities of each class label are $\{1:0.32\}$, $\{2:0.34\}$, $\{3:0.09\}$, $\{4:0.08\}$, $\{5:0.08\}$, respectively. As the probability for label 2 is the highest, the final prediction result is label 2.

RF and NB were implemented through the functions of MATLAB. RF's tree number was set to 100. SVM with Radial basis function kernel (RBF) used one-to-one strategy to deal with 5 classification problems, without parameter optimization [27].

TABLE I
THE NUMBER OF SAMPLES OF EACH CLASS OF EACH SUBJECT.

Subject	Session	Thumb	Index	Middle	Ring	Little	Total
A	A-1	209	172	198	191	189	959
	A-2	196	161	179	169	162	867
B	B-1	222	192	186	177	181	958
	B-2	204	170	193	183	185	935
	B-3	209	173	198	190	189	959
	B-4	209	173	197	191	189	959
C	C-1	167	202	196	190	203	958
	C-2	204	170	193	190	184	941
E	E-1	207	173	198	189	189	956
	E-2	207	169	197	188	185	946
	E-3	206	170	195	190	185	946
F	F-1	206	173	198	191	189	957
	F-2	208	173	198	191	189	958
	F-3	208	173	198	191	188	959
G	G-1	206	169	198	187	186	946
	G-2	209	173	197	188	188	955
H	H-1	203	167	186	184	182	922
I	I-1	209	172	198	191	189	959
	I-2	208	173	198	190	189	958

Decoding accuracy was calculated by averaging the results of 10-fold cross-validation.

III. RESULT

In this section, we first described the used dataset and the preprocessing steps, and then verified the effectiveness of frequency band selection, feature fusion, and ensemble learning. After that, we reported the final result of our method and compared it with related methods.

A. Data Description

This paper used the motor imagery EEG dataset of five fingers (5F) on the same hand including eight subjects, published by Kaya et al. [11]. The EEG data was recorded at two sampling rates of 200 Hz and 1000 Hz using an EEG-1200 JE-912 A system with 19 electrodes and 2 reference electrodes based on the international 10–20 configuration. A bandpass filter of 0.53 to 70 Hz was used for the 200 Hz data, and a bandpass filter of 0.53 to 100 Hz was used for the 1000 Hz data. A 50 Hz notch filter was also applied to both sampling rates of the data. Each subject had different sessions and each session contained 867–959 trials. Each trial lasted 2.5 to 3.5 s. In fact, the 5F dataset contains 19 sessions from eight subjects, and all 19 sessions were used in the experiments of this paper. It should be emphasized that we did not remove any trials and all trials were used in our experiments. Each trial corresponds to one sample, the sample details were shown in Table I.

Following the process of the study [11], our preprocessing steps mainly included signal downsampling, average reference, signal segmentation, and low-pass filtering. First, we downsampled all 1000 Hz data to 200 Hz. Second, the average reference was applied to the 21 channels (including 19 EEG channels and 2 reference channels). Third, each EEG epoch was extracted from the signals between 0 and 0.85 s after the onset of the visual stimulus. Finally, 30 Hz low-pass filtering was performed on the EEG data. All of the above were done using EEGLAB.

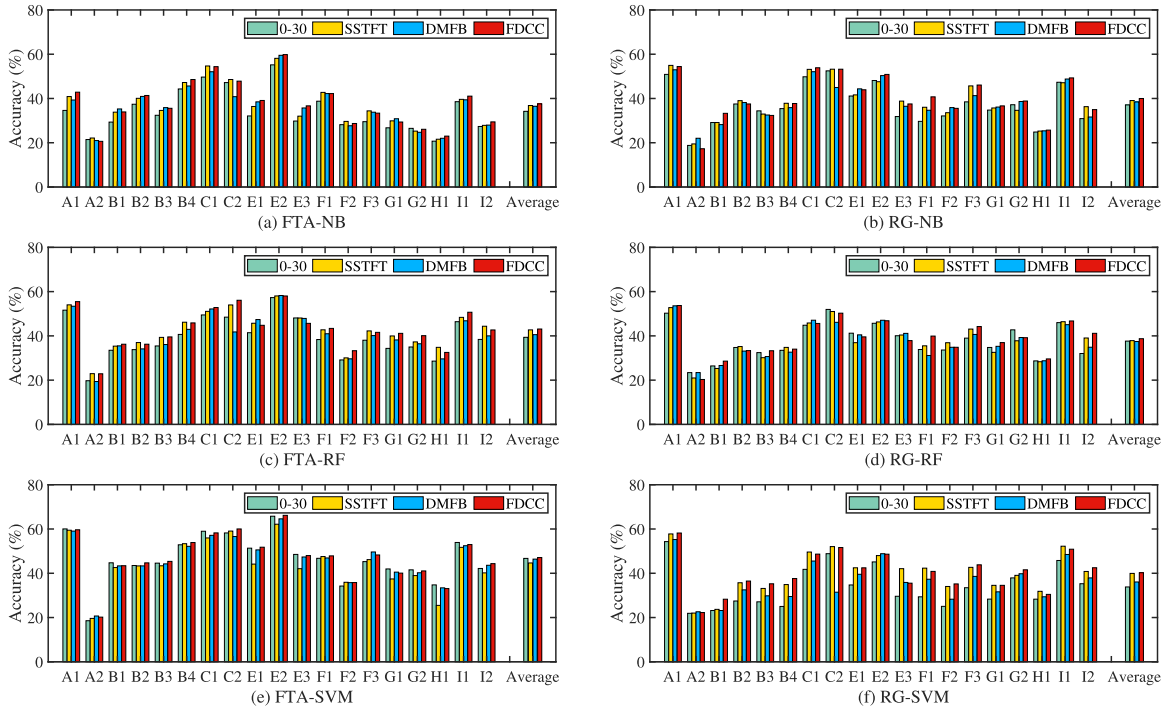

Fig. 2. Comparison of classification accuracies of SVM, RF, and NB with and without frequency band selection for each subject. (a), (c), and (e) represent the classification using FTA features. (b), (d), and (f) represent the classification using RG features. The labels on the abscissa are the subject's sessions.

B. Effectiveness of Frequency Band Selection

Most studies use EEG signals below 30 Hz to classify motor imagery tasks [28], [29], [30], [31], [32], [33], [34]. This frequency band contains mu and beta rhythms associated with event-related synchronization (ERS) and event-related desynchronization (ERD) phenomena during motor imagery [35]. Therefore, the frequency range of 0–30 Hz was targeted, and the classification accuracies before and after frequency band selection were compared to verify the effectiveness of frequency band selection. The classification result of single type feature in the 0–30 Hz band was used as a baseline. Specifically, the FDCC method was used to identify the effective frequency band of each type of feature, and then the features extracted from the identified bands were applied in classification. Two frequency band selection methods, SSTFT [21] and DMFB [22], were implemented and compared with the proposed FDCC method. The classification accuracy of each subject was shown in Fig. 2, where SVM, RF, and NB classifiers were used. The average accuracies and the results of the paired samples t-test between the FDCC method and the control methods across all sessions were shown in Table II.

The results showed our FDCC method outperformed the baseline, STFT [21] and DMFB [22] in all cases, achieving the highest average accuracy. In the case of FTA+SVM, the average accuracies of SSTFT and DMFB were 44.66% and 46.40% respectively, both worse than the baseline result of 46.72%. In the case of RG+RF, the result of DMFB was 37.46%, which was worse than the baseline result of 37.64%. Obviously, the proposed FDCC method was more effective and stable than SSTFT and DMFB.

TABLE II
COMPARISON OF AVERAGE CLASSIFICATION ACCURACY (%) AND STANDARD DEVIATION BETWEEN FDCC AND OTHER FREQUENCY BAND SELECTION METHODS.

	Method	0-30 Hz	SSTFT [21]	DMFB [22]	FDCC
FTA	SVM	46.72/10.56	44.66/10.73 **	46.40/9.88 **	**47.10/10.47**
	RF	39.36/8.95 **	42.71/8.56	40.56/9.05 **	**43.11/8.74**
	NB	34.20/9.22 **	36.82/9.98 *	36.49/9.54 *	**37.58/10.16**
RG	SVM	33.82/9.16 **	39.95/9.19	36.07/8.59 **	**40.25/.64**
	RF	37.64/7.70	37.85/8.22 *	37.46/7.78 *	**38.74/7.94**
	NB	37.09/9.01 **	39.06/9.26 *	38.44/8.57 *	**40.00/9.55**

$*p < 0.05$, $**p < 0.01$ (the paired samples t-test).

According to the hypothesis testing results in Table II, our FDCC method showed a significant improvement over the baseline in most cases. Furthermore, the FDCC method performed significantly better than DMFB, regardless of which features and classifiers were used. In addition, the FDCC method significantly outperformed SSTFT in most cases. Considering the above, the proposed FDCC is an effective and robust method.

We also compared the running time of the FDCC method and other two frequency band selection methods (all experiments were performed on the same machine configured with Intel Core i7-12700H CPU 2.3 GHz and 16 GB RAM), as shown in Table III. On average, the running time of our FDCC method for FTA features and RG features was only 1.96% and 2.3% of

TABLE III
COMPARISON OF RUNNING TIME (S) BETWEEN FDCC AND OTHER FREQUENCY BAND SELECTION METHODS

Method	SSTFT [21]	DMFB [22]	FDCC (FTA)	FDCC (RG)
Time	16.09	418.84	8.22	9.66

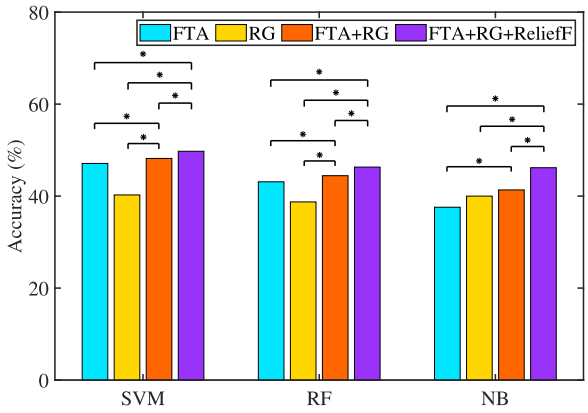

Fig. 3. Comparison of average classification accuracies of FTA, RG, FTA+RG, and FTA+RG+ReliefF. The mark $*$ indicates $p < 0.05$ (the paired samples t-test).

that of DMFB, respectively. Compared with SSTFT, our method took about half the time.

C. Effectiveness of Feature Fusion

After extracting the feature-dependent effective frequency bands, the corresponding FTA and RG features were recalculated. Each type of feature could be used as classification feature independently. Furthermore, these two types of features could be concatenated directly and used in classification, which was called simple concatenation and denoted as FTA+RG. Our method of feature fusion based on ReliefF was denoted as FTA+RG+ReliefF. Fig. 3 illustrated the classification accuracies of SVM, RF and NB with single type feature, simple concatenation and feature fusion.

It can be observed that simple concatenation achieved higher classification accuracy than single type feature in all cases. On the SVM, the p-values for FTA+RG compared with FTA and RG were 1.68×10^{-6} and 9.29×10^{-6}, respectively. On the RF, the p-values for FTA+RG compared with FTA and RG were 0.0129 and 2.81×10^{-6}, respectively. When using NB, the p-value for FTA+RG compared with FTA was 2.23×10^{-6}. These results suggested that FTA and RG features are complementary.

The feature fusion based on ReliefF could further improve the classification accuracy compared with simple concatenation. On the SVM, the classification accuracy was improved from 48.19% to 49.75%, and the p-value was 0.0029. On the RF, the classification accuracy was increased from 44.44% to 46.31%, and the p-value was 1.6×10^{-4}. The accuracy of NB was especially improved from 41.34% to 46.17%, and the p-value was 1.72×10^{-6}. These results indicated that removing redundant and interfering features can provide better results. The results also showed that the classifier performance is not equal, i.e. SVM had the best performance and RF was slightly better than NB, and it is necessary to consider the classifier weight in model.

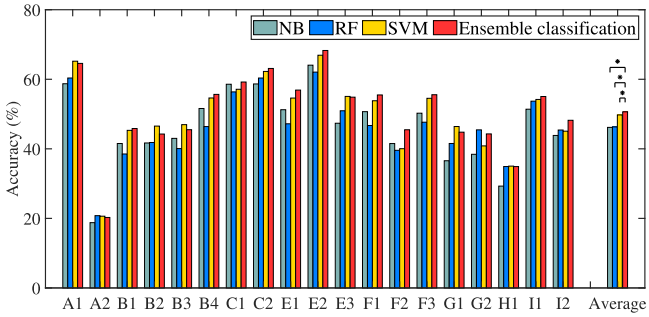

Fig. 4. Comparison of the performance between ensemble learning and individual classifier. The mark $*$ indicates $p < 0.05$ (the paired samples t-test).

D. Effectiveness of Ensemble Learning Model

We compared the results of the ensemble learning model with those of a single classifier, as shown in Fig. 4. The average classification accuracies of SVM, RF, and NB were 49.75%, 46.31%, and 46.17%, respectively, while the accuracy of the ensemble model was 50.64%, which was significantly higher than that of the single classifier (p-values of the paired samples t-test between the ensemble model with SVM, RF, and NB were 0.027, 9.70×10^{-6} and 2.28×10^{-9}, respectively). The above results showed that the ensemble model is effective.

E. Comparison With Related Studies

In this paper, the proposed DSFE method achieved the final classification accuracy of 50.64% with a standard deviation of 10.88%. For comparison, the previous results of finger motor imagery taken directly from studies [11], [13], [14], [36] were presented. Furthermore, three competitive deep learning methods (i.e. AMCNN-DGCN [37], RGNN [38] and FBN-CNN [39]) were reproduced in this paper according to the settings described in the original literature for comparison. Since power spectral density (PSD) is an important feature of EEG motor imagery, the additional classification experiments of SVM, RF and NB based on PSD features were also performed. Table IV showed the comparison of results between our method and existing methods. On the all samples (i.e. trial) of this dataset, our method achieved 7.64% and 10.04% improvement over the methods of kaya [11] and kato [13]. Azizah [14] deleted EEG trials with a signal-to-noise ratio below zero, then used spectrogram and SVM to achieve a classification accuracy of 46.7%. Although we did not remove any trial, the decoding accuracy of our method was still 3.94% higher than that of Azizah.

The paired samples t-test between our method and studies [13] and [14] showed that our DSFE method has a significant performance improvement. On the other hand, our method achieved higher average accuracy than these deep learning approaches, including sub-segment Net [36], ViT [36], AMCNN-DGCN [37],

TABLE IV
COMPARISON OF CLASSIFICATION ACCURACY (%) BETWEEN THE PROPOSED DSFE METHOD AND OTHER METHODS.

Session	FTA+ SVM [11]	CSP+SVM [13]	Spectrogram+ SVM [14]	PSD+SVM	PSD+RF	PSD+NB	Sub-segment Net [36]	ViT [36]	AMCNN-DGCN [37]	RGNN [38]	FBN-CNN [39]	DSFE
A-1		58.3	59.3	25.23	49.23	22.22	–	–	49.43	36.39	51.31	64.57
A-2		21.7	20.8	23.30	20.76	23.64	23.38	25.87	26.64	24.34	28.60	20.27
B-1		39.2	43.1	22.96	27.06	21.93	–	–	33.92	25.16	46.02	45.84
B-2		40.2	42.5	22.36	28.77	26.21	44.68	26.38	42.57	24.70	45.67	44.26
B-3		39.2	44.1	21.27	29.19	21.38	47.10	27.03	37.95	25.35	45.89	45.50
B-4		50.6	53.9	22.94	31.29	28.49	–	–	45.05	24.62	46.08	55.66
C-1		56.4	61.4	22.96	38.73	29.24	–	–	43.11	29.44	50.41	59.22
C-2		51.2	61.7	21.89	43.02	32.50	55.60	19.92	46.32	35.07	49.52	63.11
E-1		43.4	52.3	21.65	32.22	21.22	54.69	41.80	46.54	26.14	50.52	56.90
E-2		52.9	66.5	21.88	37.32	24.34	68.29	59.76	51.26	28.33	50.10	68.28
E-3		42.4	53.0	21.78	32.14	23.57	63.82	53.66	42.61	26.85	51.38	54.86
F-1		30.0	38.6	21.53	24.85	21.21	–	–	39.30	25.71	49.54	55.50
F-2		38.1	34.1	21.71	22.96	21.10	–	–	32.37	23.50	48.62	45.49
F-3		41.8	45.4	23.36	27.84	21.79	40.15	41.31	38.58	26.59	50.26	55.56
G-1		36.5	41.6	21.99	25.99	18.70	44.31	33.33	39.01	29.71	47.66	44.79
G-2		33.3	42.4	22.62	27.01	20.73	43.14	24.71	39.99	26.39	49.94	44.29
H-1		23.9	34.0	22.02	32.01	18.11	39.64	22.07	33.19	27.77	51.29	34.90
I-1		43.3	51.4	22.11	39.83	21.16	55.60	51.74	46.41	28.05	50.06	55.05
I-2		28.4	41.7	22.44	31.76	19.62	49.22	45.35	41.97	24.63	48.32	48.21
Mean/std	43/10.0	40.6/10.06	46.7/11.01	22.42/0.89	31.68/7.0	23.01/3.63	48.43/11.12	36.38/12.81	40.85/6.10	27.30/3.35	47.96/4.93	**50.64/10.88**
p (value)		6.69e-7	7.48e-4	9.91e-10	2.52e-9	4.04e-10			1.55e-6	2.52e-9	0.089	

[11] reported the average result. [14] removed the trials of low signal-to-noise ratio. [36] reported the results of partial sessions. The paired samples t-test was used to determine the significant difference between our DSFE method and other methods.

RGNN [38] and FBN-CNN [39], with accuracy improvements of 2.21%, 14.26%, 9.79%, 23.34% and 2.69%, respectively.

F. Classification Confusion Matrix

The classification confusion matrix in one fold of the DSFE method for each subject were shown as examples in Fig. 5. Through the confusion matrices, we found that thumb and little finger were easy to distinguish, index finger was easy to be misclassified as thumb, and ring finger was easy to be misclassified as little finger. This result suggested that adjacent fingers are more susceptible to misclassification. One possible reason for the difficulty in discriminating adjacent fingers is that the neural activity associated with adjacent fingers occurs in very close or even overlapping areas during finger motor imagery. Similar views have been reported in previous studies [13], [40].

IV. DISCUSSION

In this paper, we proposed a feature-dependent frequency band selection method (FDCC) that can improve the decoding accuracy for finger motor imagery tasks. We counted the effective frequency bands of the specific feature for each subject identified by the FDCC method to investigate the characteristics of the effective frequency bands across different subjects and across different features. Due to slight differences between the results of different folds in the process of 10-fold cross-validation, the frequency bands with the maximum selection probability by different methods for each subject were shown in Table V.

It can be seen from Table V that the effective frequency bands were different for different subjects. For example, the width of the selected FTA-specific frequency band of subject H1 was more than twice that of subject A1 (0–26 Hz vs. 0–12 Hz), while the RG-specific effective frequency band of subject B2 was 0–4 Hz and that of subject E2 was 0–14 Hz. We also observed

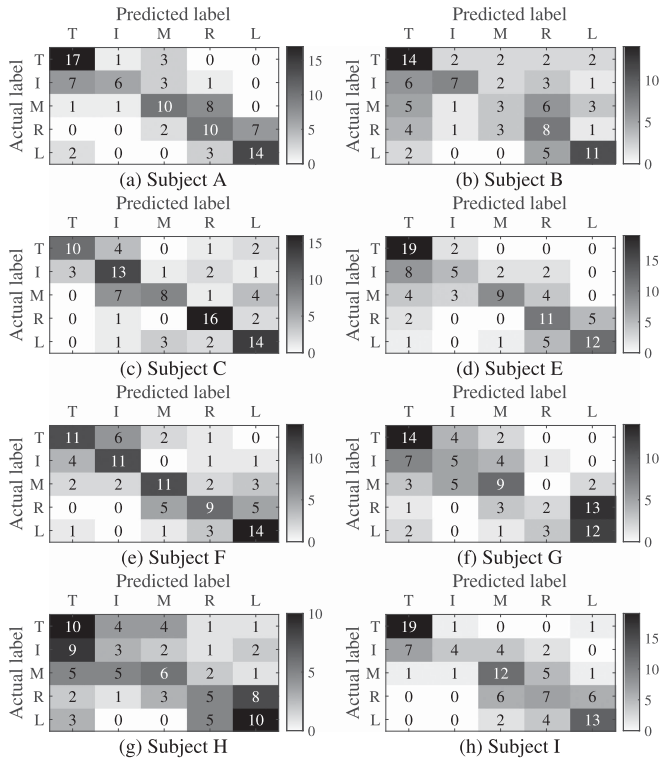

Fig. 5. Classification confusion matrix of each subject. (a)–(h) A1, B4, C2, E2, F1, G1, H1 and I1 were selected as examples. T: Thumb, I: Index, M: Middle, R: Ring, L: Little.

a remarkable phenomenon: the effective frequency band of the FTA features was generally wider than that of the RG features. This result illustrated that the effective frequency bands of different types of features were also different. In addition, the effective frequency bands selected by the two contrast methods on

TABLE V
FREQUENCY BANDS (HZ) SELECTED FOR DIFFERENT SUBJECTS.

Subject	Session	SSTFT [21]	DMFB [22]	FDCC(FTA)	FDCC(RG)
A	1	0-9	0-20	0-12	0-8
	2	0-10	4-24	2-8	10-12
B	1	0-11	0-16	0-16	0-6
	2	0-11	0-14	0-24	0-4
	3	0-11	0-16	0-16	0-6
	4	0-13	0-18	0-26	0-6
C	1	0-12	0-18	0-18	0-4
	2	0-12	4-18	0-28	0-6
E	1	0-9	0-16	0-22	0-8
	2	0-13	0-16	0-22	0-14
	3	0-11	0-16	0-20	0-2
F	1	0-15	0-14	2-10	0-8
	2	0-13	0-16	2-8	0-6
	3	0-13	0-16	0-14	0-8
G	1	0-8	0-12	0-14	0-6
	2	0-7	0-18	0-12	0-6
H	1	0-7	0-20	0-26	0-8
I	1	0-8	0-20	0-20	0-6
	2	0-8	0-20	0-24	0-4

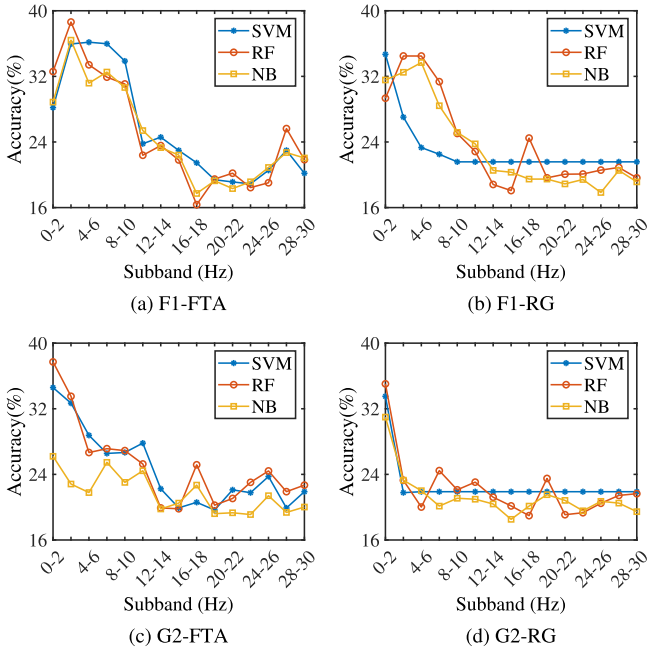

Fig. 6. Classification performance of each subband of subjects F1 and G2.

different subjects were also different. This was consistent with the conclusion of our FDCC method. However, their methods are feature-independent and cannot select effective frequency bands for specific features.

We further used the classification performance of each subband of width 2 Hz to check the selected frequency band of the FDCC method: target features from each of 15 non-overlapping subbands were used in a 10-fold cross-validation classification experiment. Subjects F1 and G2 were selected as examples, and the results were shown in Fig. 6. For subject F1, it can be seen that the peak accuracy of the FTA features occurred in the 2–10 Hz range (Fig. 6(a)), which was consistent with the 2–10 Hz band identified by FDCC and did not match the 0–15 Hz and 0–14 Hz bands identified by the contrast SSTFT and DMFB methods. Similarly, the accuracy of the RG features was very low after 8 Hz, consistent with the 0–8 Hz band chosen by FDCC, but the 0–15 Hz and 0–14 Hz bands of SSTFT and DMFB contained many subbands with poor performance. Fig. 6(c) showed that subject G2's FTA features presented a significant drop in classification accuracy after 12 Hz, which was consistent with the 0–12 Hz band selected by FDCC, but inconsistent with the 0–7 Hz and 0–18 Hz of the two contrast methods. The above results showed that our FDCC method can identify the feature-dependent effective frequency band for each subject more accurately than the two contrast methods.

A previous study has shown that the effective frequency bands of ordinary motor imagery tasks (such as left hand and right hand) are mainly mu band (8–13 Hz) and beta band (13–30 Hz) [35]. The RG features of this frequency range have been used wildly in classification [41], [42]. However, for the finger motor imagery task, the effective frequency bands of FTA features and RG features identified by the FDCC method were mainly 0–20 Hz and 0–8 Hz, respectively (Table V). Obviously, for the RG features, there was a very large difference between the effective frequency band of finger motor imagery and that of two-hand motor imagery. Compared with two-hand motor imagery, the effective decoding information of the RG features of finger motor imagery was shifted to low frequencies. To further verify this, we designed a comparative experiment between these two motor imagery tasks by introducing another public dataset of left-right hands.

We chose a widely used left-right hands motor imagery dataset BCIC IV 2b [43] for our experiment. This dataset consists of EEG data from 9 subjects with three channels (C3, Cz, and C4). The motor imagery task lasted for 4 seconds. We extracted EEG data of 0 to 3 seconds after the visual stimuli and decomposed the data into six frequency bands: delta (0.5–4 Hz), theta (4–8 Hz), alpha (8–13 Hz), beta1 (13–20 Hz), beta2 (20–25 Hz), and beta3 (25–30 Hz). The FTA and RG features on each frequency band were extracted as classification features, and the classification accuracy was calculated in a 10-fold cross-validation subject-dependent experiment of mixing predefined training and test samples. Similarly, we conducted a consistent experiment on the finger motor imagery dataset. To avoid the influence of the number of channels, we only used EEG data with C3, Cz and C4 channels.

The average accuracies of all subjects in the comparative experiment were shown in Fig. 7. It can be seen that the alpha and beta2 bands produced a high classification accuracy for two-hand motor imagery task (Fig. 7(a) and (b)), which was consistent with existing research. However, for finger motor imagery, the highest classification accuracies occurred in the delta and theta bands, i.e. effective discriminative information related to finger motor imagery task was roughly concentrated in the low frequency band below 8 Hz (Fig. 7(c) and (d)). Moreover, the fact that the effective frequency band of the finger motor imagery was shifted to a lower frequency is more evident in the RG features than in the FTA features. These results suggested that there may be a great difference in the internal mechanism between finger motor imagery tasks and two-hand motor imagery. At the same time, these results provided evidence

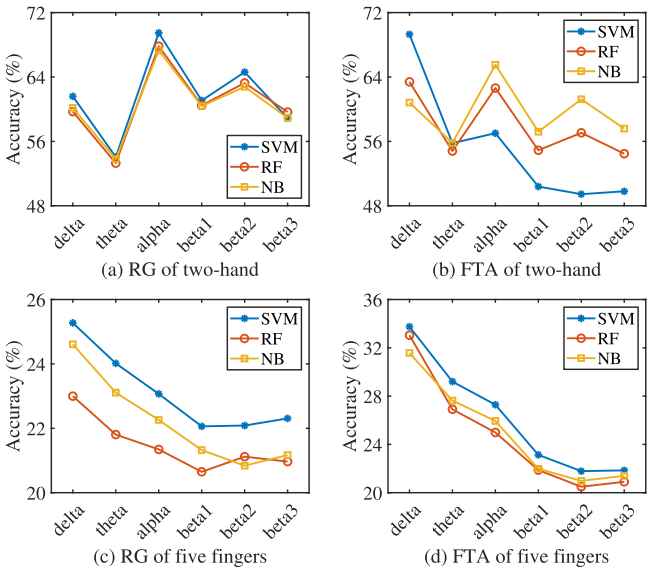

Fig. 7. Comparison of classification accuracies between two-hand motor imagery and finger motor imagery on different frequency bands.

that studying the feature-dependent effective frequency bands is a powerful means of exploring the mysteries of finger motor imagery.

This paper proposed a novel EEG decoding method (DSFE) for finger motor imagery, which combines feature-dependent frequency band selection, feature fusion and ensemble learning. Although three steps are closely linked to fulfil their respective functions, each step can be flexibly adjusted to specific tasks and needs, such as introducing additional task-relevant effective features, adding or replacing classification methods, etc. An outstanding advantage of the DSFE method is that the idea is novel and the implementation is intuitive, so that the results are highly interpretable. The DSFE method can provide very valuable information for an in-depth study of the characteristics of EEG signals for specific task. For example, the results of the DSFE method revealed that the effective decoding information of finger motor imagery is transferred to the lower frequency compared with two-hand motor imagery. Recently, deep learning has been widely applied to EEG data to automatically capture features due to its good performance. However, the features captured by deep learning are difficult to interpret. In the future, deep learning can be incorporated based on the proposed DSFE method. Of course, more data needs to be tested by the DSFE method.

V. Conclusion

In this work, we proposed the DSFE method to decode the EEG data of finger motor imagery based on feature-dependent effective frequency band selection, feature fusion, and ensemble learning. The results on the public dataset showed that the proposed method effectively improves the decoding performance of five fingers motor imagery and achieves the accuracy of 50.64%. The experiments further revealed that both the effective frequency bands of different subjects and the effective frequency bands of different types of features are different in finger motor imagery. Furthermore, compared with two-hand motor imagery, the effective decoding information of finger motor imagery is transferred to the lower frequency. The idea and findings in this paper provide a possible perspective for understanding fine motor imagery in-depth. Finally, the method presented in this paper can be easily adapted or directly applied in other EEG tasks.

References

[1] J. R. Wolpaw et al., "Brain–computer interfaces for communication and control," *Clin. Neuriophysiol.*, vol. 113, no. 6, pp. 767–791, 2002.
[2] A. N. Belkacem et al., "Brain computer interfaces for improving the quality of life of older adults and elderly patients," *Front. Neurosci.*, vol. 14, 2020, Art. no. 692.
[3] O. George, R. Smith, P. Madiraju, N. Yahyasoltani, and S. I. Ahamed, "Motor imagery: A review of existing techniques, challenges and potentials," in *Proc. IEEE 45th Annu. Comput., Softw., Appl. Conf.*, 2021, pp. 1893–1899.
[4] G. Pfurtscheller and C. Neuper, "Motor imagery and direct brain-computer communication," in *Proc. IEEE*, vol. 89, no. 7, Jul. 2001, pp. 1123–1134.
[5] A. Al-Saegh, S. A. Dawwd, and J. M. Abdul-Jabbar, "Deep learning for motor imagery EEG-based classification: A review," *Biomed. Signal Process. Control*, vol. 63, 2021, Art. no. 102172.
[6] C. Brunner, M. Billinger, M. Seeber, T. R. Mullen, and S. Makeig, "Volume conduction influences scalp-based connectivity estimates," *Front. Comput. Neurosci.*, vol. 10, 2016, Art. no. 121.
[7] F. Quandt et al., "Single trial discrimination of individual finger movements on one hand: A combined MEG and EEG study," *NeuroImage*, vol. 59, no. 4, pp. 3316–3324, 2012.
[8] R. Xiao and L. Ding, "EEG resolutions in detecting and decoding finger movements from spectral analysis," *Front. Neurosci.*, vol. 9, 2015, Art. no. 308.
[9] T. Hayashi, H. Yokoyama, I. Nambu, and Y. Wada, "Prediction of individual finger movements for motor execution and imagery: An EEG study," in *Proc. IEEE Int. Conf. Systems, Man, Cybern.*, 2017, pp. 3020–3023.
[10] J. B. Salyers, Y. Dong, and Y. Gai, "Continuous wavelet transform for decoding finger movements from single-channel EEG," *IEEE Trans. Biomed. Eng.*, vol. 66, no. 6, pp. 1588–1597, Jun. 2019.
[11] M. Kaya et al., "A large electroencephalographic motor imagery dataset for electroencephalographic brain computer interfaces," *Sci. Data*, vol. 5, pp. 1–16, 2018.
[12] K. Anam, M. Nuh, and A. Al-Jumaily, "Comparison of EEG pattern recognition of motor imagery for finger movement classification," in *Proc. IEEE 6th Int. Conf. Elect. Eng., Comput. Sci. Inform.*, 2019, pp. 24–27.
[13] M. Kato et al., "Motor imagery classification of finger motions using multiclass CSP," in *Proc. IEEE 42nd Annu. Int. Conf. IEEE Eng. Med. Biol. Soc.*, 2020, pp. 2991–2994.
[14] R. N. Azizah, H. Zakaria, and B. R. Hermanto, "Channels selection for pattern recognition of five fingers motor imagery electroencephalography signals," *J. Phys.: Conf. Ser.*, vol. 2312, no. 1, 2022, Art. no. 0 12019.
[15] K. Anam, S. Bukhori, F. S. Hanggara, and M. Pratama, "Subject-independent classification on brain-computer interface using autonomous deep learning for finger movement recognition," in *Proc. IEEE 42nd Annu. Int. Conf. Eng. Med. Biol. Soc.*, 2020, pp. 447–450.
[16] T. Mwata-Velu et al., "Imaginary finger movements decoding using empirical mode decomposition and a stacked BiLSTM architecture," *Mathematics*, vol. 9, no. 24, 2021, Art. no. 3297.
[17] H. S. Lee et al., "Individual finger movement decoding using a novel ultra-high-density electroencephalography-based brain-computer interface system," *Front. Neurosci.*, vol. 16, 2022, Art. no. 1009878
[18] Z. Ma, M. Xu, K. Wang, and D. Ming, "Decoding of individual finger movement on one hand using ultra high-density EEG," in *Proc. IEEE 16th ICME Int. Conf. Complex Med. Eng.*, 2022, pp. 332–335.
[19] G. Pfurtscheller, B. Graimann, J. Huggins, S. Levine, and L. Schuh, "Spatiotemporal patterns of beta desynchronization and gamma synchronization in corticographic data during self-paced movement," *Clin. Neuriophysiol.*, vol. 114, no. 7, pp. 1226–1236, 2003.
[20] Y. Hashimoto and J. Ushiba, "EEG-based classification of imaginary left and right foot movements using beta rebound," *Clin. Neuriophysiol.*, vol. 124, no. 11, pp. 2153–2160, 2013.

[21] D. Delisle-Rodriguez et al., "System based on subject-specific bands to recognize pedaling motor imagery: Towards a BCI for lower-limb rehabilitation," *J. Neural Eng.*, vol. 16, no. 5, 2019, Art. no. 0 56005.
[22] F. Wu, A. Gong, H. Li, L. Zhao, W. Zhang, and Y. Fu, "A new subject-specific discriminative and multi-scale filter bank tangent space mapping method for recognition of multiclass motor imagery," *Front. Hum. Neurosci.*, vol. 15, 2021, Art. no. 595723.
[23] M. S. Yamamoto, F. Lotte, F. Yger, and S. Chevallier, "Class-distinctiveness-based frequency band selection on the Riemannian manifold for oscillatory activity-based BCIs: Preliminary results," in *Proc. IEEE 44th Annu. Int. Conf. Eng. Med. Biol. Soc.*, 2022, pp. 3690–3693.
[24] A. Barachant et al., "Multiclass brain–computer interface classification by Riemannian geometry," *IEEE Trans. Biomed. Eng.*, vol. 59, no. 4, pp. 920–928, Apr. 2012.
[25] K. Kira and L. A. Rendell, "A practical approach to feature selection," in *Proc. Mach. Learn. Proc.*, 1992, pp. 249–256.
[26] I. Kononenko, "Estimating attributes: Analysis and extensions of RELIEF," in *Proc. Mach. Learn.*, 1994, pp. 171–182.
[27] C.-C. Chang and C.-J. Lin, "LIBSVM: A library for support vector machines," *ACM Trans. Intell. Syst. Technol.*, vol. 2, no. 3, pp. 1–27, 2011.
[28] C. Silva, R. Duarte, and A. Trofino, "Feature extraction improvements using an LMI approach and riemannian geometry tools: An application to BCI," in *Proc. IEEE Conf. Control Appl.*, 2016, pp. 966–971.
[29] X. Xie, Z. L. Yu, H. Lu, Z. Gu, and Y. Li, "Motor imagery classification based on bilinear sub-manifold learning of symmetric positive-definite matrices," *IEEE Trans. Neural Syst. Rehabil. Eng.*, vol. 25, no. 6, pp. 504–516, Jun. 2017.
[30] D. Gurve, D. Delisle-Rodriguez, T. Bastos, and S. Krishnan, "Motor imagery classification with covariance matrices and non-negative matrix factorization," in *Proc. IEEE 41st Annu. Int. Conf. Eng. Med. Biol. Soc.*, 2019, pp. 3083–3086.
[31] Y. Chu et al., "Decoding multiclass motor imagery EEG from the same upper limb by combining riemannian geometry features and partial least squares regression," *J. Neural Eng.*, vol. 17, no. 4, 2020, Art. no. 0 46029.
[32] F. Qi et al., "Spatiotemporal-filtering-based channel selection for single-trial EEG classification," *IEEE Trans. Cybern.*, vol. 51, no. 2, pp. 558–567, Feb. 2021.
[33] H. Varsehi and S. M. P. Firoozabadi, "An EEG channel selection method for motor imagery based brain–computer interface and neurofeedback using granger causality," *Neural Netw.*, vol. 133, pp. 193–206, 2021.
[34] J. Yu and Z. L. Yu, "Cross-correlation based discriminant criterion for channel selection in motor imagery BCI systems," *J. Neural Eng.*, vol. 18, no. 4, 2021, Art. no. 0 46083.
[35] G. Pfurtscheller et al., "Mu rhythm (de)synchronization and EEG single-trial classification of different motor imagery tasks," *NeuroImage*, vol. 31, no. 1, pp. 153–159, 2006.
[36] P. Zhou, Q. Ye, H. Luo, and Z. Lu, "Finger motor imagery based on optimal sub-segment deep learning research on EEG signal classification," *Appl. Res. Comput.*, vol. 59, no. 05, pp. 160–168, 2023.
[37] H. Wang, L. Xu, A. Bezerianos, C. Chen, and Z. Zhang, "Linking attention-based multiscale CNN with dynamical GCN for driving fatigue detection," *IEEE Trans. Instrum. Meas.*, vol. 70, pp. 1–11, 2021.
[38] P. Zhong, D. Wang, and C. Miao, "EEG-based emotion recognition using regularized graph neural networks," *IEEE Trans. Affect. Comput.*, vol. 13, no. 3, pp. 1290–1301, Jul.–Sep. 2022.
[39] J. Chen et al., "Two-dimensional phase lag index image representation of electroencephalography for automated recognition of driver fatigue using convolutional neural network," *Expert Syst. With Appl.*, vol. 191, 2022, Art. no. 116339.
[40] R. Alazrai, M. Abuhijleh, H. Alwanni, and M. I. Daoud, "A deep learning framework for decoding motor imagery tasks of the same hand using EEG signals," *IEEE Access*, vol. 7, pp. 109612–109627, 2019.
[41] S. Guan, K. Zhao, and S. Yang, "Motor imagery EEG classification based on decision tree framework and Riemannian geometry," *Comput. Intell. Neurosci.*, vol. 2019, 2019, Art. no. 5627156.
[42] H. He and D. Wu, "Transfer learning for brain–computer interfaces: A Euclidean space data alignment approach," *IEEE Trans. Biomed. Eng.*, vol. 67, no. 2, pp. 399–410, Feb. 2020.
[43] R. Leeb, C. Brunner, G. Müller-Putz, A. Schlögl, and G. Pfurtscheller, "BCI competition 2008–Graz data set B," Graz University of Technology, Austria, vol. 16, pp. 1–6, 2008.